Article:
Zhu, H, Yang, Y, Hyeon-Deuk, K et al. (6 more authors) (2014) Auger-assisted electron transfer from photoexcited semiconductor quantum dots. Nano Letters, 14 (3). pp. 1263-1269. ISSN 1530-6984

https://doi.org/10.1021/nl4041687

Auger-Assisted Electron Transfer from Photoexcited Semiconductor Quantum Dots

Authors: Haiming Zhu,[1#] Ye Yang,[1#] Kim Hyeon-Deuk,[2] Marco Califano,[3] Nianhui Song,[1] Youwei Wang,[4] Wengqing Zhang,[4] Oleg V. Prezhdo,[5] Tianquan Lian[1*]

Affiliations:

1 Department of Chemistry, Emory University, Atlanta, Georgia, 30322, USA.

2 Department of Chemistry, Kyoto University, Kyoto, 606-8502, and Japan Science and Technology Agency, PRESTO, 4-1-8 Honcho, Kawaguchi, Saitama, 332-0012, Japan

3 Institute of Microwaves and Photonics, School of Electronic and Electrical Engineering, University of Leeds, Leeds LS2 9JT, United Kingdom.

4. State Key Laboratory of High Performance Ceramics and Superfine Microstructure, Shanghai Institute of Ceramics, Chinese Academy of Sciences, Shanghai 200050, China

5. Department of Chemistry, University of Rochester, Rochester, NY 14642, USA

# These authors contribute equally to this work.

Abstract

Although quantum confined nanomaterials, such as quantum dots (QDs) have emerged as a new class of light harvesting and charge separation materials for solar energy conversion, theoretical models for describing photoinduced charge transfer from these materials remains unclear. In this paper, we show that the rate of photoinduced electron transfer from QDs (CdS, CdSe and CdTe) to molecular acceptors (anthraquinone, methylviologen and methylene blue) increases at decreasing QD size (and increasing driving force), showing a lack of Marcus inverted regime behavior over an apparent driving force range of ~ 0-1.3 V. We account for this unusual driving force dependence by proposing an Auger-assisted electron transfer model, in which the transfer of the electron can be coupled to the excitation of the hole, circumventing the unfavorable Frank-Condon overlap in the Marcus inverted regime. This model is supported by computational studies of electron transfer and trapping processes in model QD-acceptor complexes.

Keywords: quantum dots, transient absorption spectroscopy, electron transfer, Auger, Marcus theory

In recent years, quantum confined semiconductor nanomaterials, such as quantum dots (QDs), nanorods and carbon nanotubes, have emerged as a new class of light harvesting and charge separation materials for solar energy conversion.[1-8] For these applications, one of the most fundamental and crucial steps is the dissociation of excitons (bound electron-hole pairs) in these materials through interfacial charge (electron or hole) transfer to acceptor materials. Due to the strong electron-nuclear interaction in molecules, inter- and intra- molecular electron transfer (ET) is accompanied by large rearrangement of the nuclear configuration, which are described by the Marcus ET theory,[9-12] exhibiting the well-known dependences of ET rates on the driving force in the Marcus normal, barrier-less, and inverted regimes.[10,13,14] In many bulk semiconductor materials (such as CdX, X=S, Se, and Te), the week electron-nuclear and electron-electron interaction justify the treatment of electrons and holes as quasi-free and independent particles, in which photoinduced electron transfer requires negligible change in nuclear configurations or the motion of the accompanying holes.[15] In excitonic nanomaterials, such as QDs, both the electron-hole interaction and electron-phonon interactions fall between those of the bulk semiconductor materials and molecular chromophores and the appropriate model for describing photoinduced charge transfer (or exciton dissociation) remains unclear.

In an effort to test theoretical models for describing ET from excitonic nanomateirals, in this paper, we investigate electron transfer in QD-molecular complexes. Because of the quantum confinement effect, semiconductor QDs exhibit atomic-like discrete electronic levels and corresponding excitonic transitions that can be widely tuned by their size.[16,17] Such size dependent energetics provides an ideal platform for testing ET models. In a recent study of ET from QDs to metal oxide films, it was shown that ET rates increase at larger driving force even when it far exceeds the reorganization energy.[18-20] This trend was attributed to the existence of a

continuum of conduction band states and their increasing density at higher energy in metal oxides, similar to previous reports for ET from molecules to oxides.[21,22] Previous studies of ET in QD-acceptor complexes have also reported faster ET rates at smaller QD size.[23] Unfortunately, the range of driving force was limited and a critical test of ET models has not been possible.

In this study, we investigate the size dependence of ET processes from CdS, CdSe and CdTe QDs to three molecular acceptors, methylene blue (MB^+), methyl viologen (MV^{2+}) and anthraquinone (AQ), as shown in Figure 1A. The combination of band edges of bulk materials, size tunable confinement energies, and acceptor redox potentials ($\emptyset_{A/A^-}$: 4.7 V (*vs* vacuum),[24,25] MV^{2+} ~ -4.26 V[26] and AQ ~ -4 V[27]) enables an examination of ET rates over an apparent driving force range of ~ 0 - 1.3 eV (energy gap between the lS electron and the adsorbate LUMO). The observed ET rates increase with decreasing QD size, regardless of QD compositions and acceptor redox potentials, in marked contrast with the conventional ET model currently used in the literature. We propose an Auger-assisted model for ET from QDs, in which the excess energy of the electron can be conserved by hole excitation, overcoming the unfavorable Franck-Condon overlap in the Marcus inverted regime and enhancing the ET rate. This model can satisfactorily explain the observed size dependent ET rates and is supported by theoretical/computational modeling.

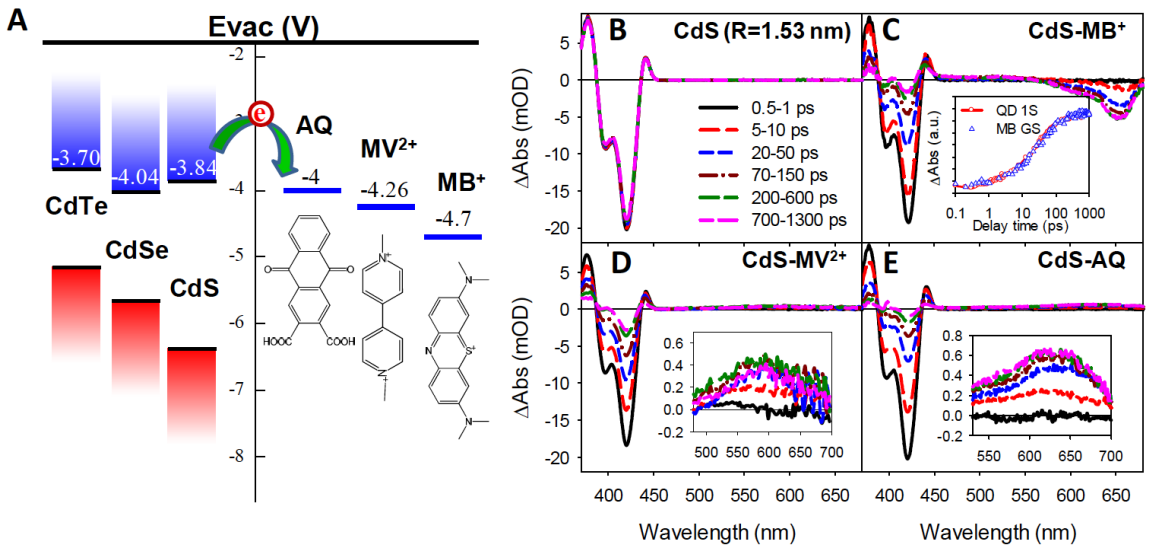

Figure 1. (A) Schematic diagram of bulk conduction band edge positions of CdX (X=S, Se, Te) *(12, 13)* and reduction potentials of acceptor molecules (*vs* vacuum).(*14-16*) The schematic structures of acceptor molecules are also shown. (B,C,D,E) Representative TA spectra of (B) free CdS QDs (R=1.53 nm), (C) CdS-MB^+ complexes, (D) CdS-MV^{2+} complexes, and (E) CdS-AQ complexes at indicated delay time windows after 400 nm excitation. (Inset in C) Comparison of QD 1S bleach recovery kinetics (red circles) and the MB^+ GS bleach formation kinetics (blue triangles) in CdS-MB^+ complexes. The MB^+ GS bleach signal has been normalized and inverted for better comparison. (Inset in D and E) expanded views of the spectra at 500−700 nm showing the formation of radicals.

The syntheses of Oleic acid (OA) capped CdS, CdSe and CdTe QDs of different sizes are described in the Supporting Information (SI1) and their UV-Vis absorption spectra are shown in Figure S1. From the effective mass modeling (SI2) as well as an empirical sizing curve[28], the radius of these synthesized QDs can be determined to be in the range of 1 ~ 2.2 nm. QD-molecular acceptor (MB^+, MV^{2+}, AQ) complexes with desired adsorbate-to-QD ratios were

prepared in heptane solution for time resolved transient absorption (TA) spectroscopic measurements (See SI1 for experimental details). Representative TA spectra of CdS (radius R = 1.53 nm) QDs and their complexes with MB^+, MV^{2+} and AQ are shown in Figure 1 (Similar spectra for CdSe (R = 1.53 nm) and CdTe (R = 1.59 nm) QDs are shown in Figure S3). All samples are measured at low excitation fluence to ensure negligible contributions of multi-exciton states. As shown in Figure 1, the TA spectra of free CdS QDs consist of a long-lived bleach of 1S exciton band due to the state filling of the 1S electron level and derivative like features caused by the presence of the exciton.[29] The spectra of CdS-MB^+ complexes show a much faster 1S exciton bleach recovery (compared with free QDs without molecular acceptors) that is accompanied by the formation of the bleach of MB^+ ground state (GS) absorption at ~650 nm with same kinetics (Figure 1C inset).[25,30] For the CdS-MV^{2+} and CdS-AQ complexes, the recovery of 1S bleach is accompanied by the formation of reduced adsorbates ($MV^{+\cdot}$ and AQ^- radicals) signals at ~600 nm and ~630 nm, respectively (Figure 1D and 1E).[29,31-33] Therefore, the photoinduced ET processes from the excited QDs to adsorbates can be monitored by the kinetics of either the QD (1S exciton bleach recovery) or adsorbate (ground state bleach or radical formation) TA features, as shown in Figure S4.

QD-acceptor ET rates depend on the number of acceptors per QD, whose distribution is governed by Poisson statistics.[29,34,35] To compare ET rates among different QD-acceptor complexes with different ratios, we determine an "intrinsic" ET rate (k_I) in 1:1 complexes from the measured ET kinetics (see supporting information SI5). The intrinsic ET rates for all QD-acceptor complexes are listed in Table S2 and plotted as a function of radius in Figure S4. For reason yet to be understood, the ET times from CdSe QDs to MV^{2+} are <100 fs and cannot be reliably extracted to examine its size dependence and are not included in this study.

We first examine how ET rates depend on the size of QDs within each series of QD-acceptor complexes. The intrinsic ET rates are plotted as a function of QD size for CdS, CdSe and CdTe in Figure 2A, 2B and 2C, respectively. Because of the large variation of ET rates to different acceptors, to facilitate comparison, the rate constants have been scaled to have similar values for the smallest QDs in each QD-acceptor series. The scaling factors for each QD-acceptor series are listed in the figures. For all QD-acceptor complexes, ET rate increases with decreasing QD size, regardless of the QD compositions and molecular acceptors. The size dependence is more pronounced for AQ compared to MB^+. For example, decreasing the CdS radius from 2.2 to 1.2 nm, the ET rate constant increases by ~ 350 folds for AQ, ~ 25 folds for MV^{2+} and ~10 folds for MB^+.

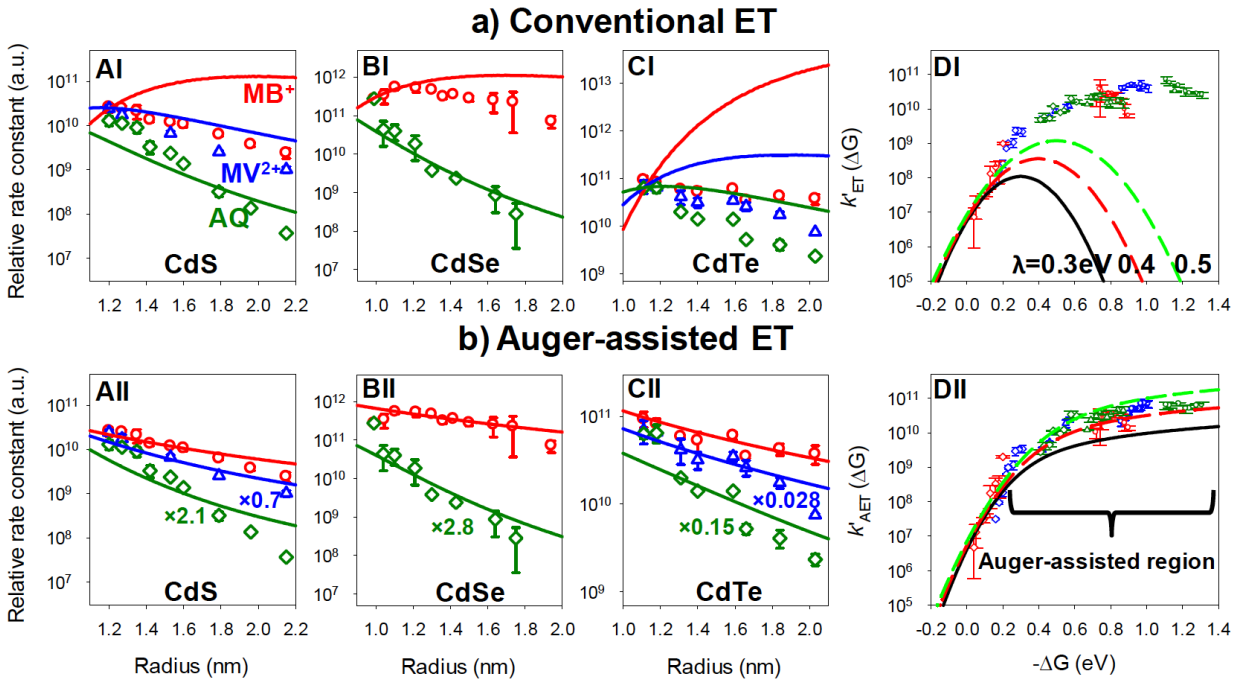

Figure 2. (A-C) Measured size-dependent ET rates (symbols) of CdS (Ai) CdSe (Bi) and CdTe (Ci) QDs to MB^+ (red circles), MV^{2+} (blue triangle), and AQ (green diamond), and theoretical

fits (solid line) calculated assuming λ = 0.4 V according to the conventional (Eq. 1, i=I, upper panles) and Auger-assisted (Eq. 3, i=II, lower panels) ET models. ET rate constants to different acceptors have been scaled to have similar values for the smallest size of QDs and the scaling factors are indicated in the figure. (D) Measured (symbols) and predicted (lines) ET rates as a function of driving force according to the conventional (DI) and Auger-assisted (DII) ET models. The predicted values are calculated according to Eq. 4 and 5 with λ values of 0.3 (black solid line), 0.4 (red dashed line), 0.5 (green dashed line) eV. The measured ET rate constants of from CdX QDs (CdS: blue, CdSe: red, CdTe: dark green) to molecular acceptors (MB^+: circles, MV^{2+}: triangles, AQ: diamonds) have been scaled by the R dependent prefactors in Eq. S12 ($C_H|\Psi_{1Se}(R)_0|^2$) and Eq. S13 ($C|\Psi_{1Se}(R)_0|^2R^2$), respectively, to account for the size and materials dependent variation of coupling strength. The C and C_H values for each series of QD-acceptor complexes are chosen such that QD-acceptors with the same driving force have the same scaled ET rates regardless of their chemical nature.

In the conventional ET model that is widely used in QD electron transfer study,[18,19,31] it is assumed that as the 1S electron is transferred from the excited QD (QD*) to the acceptor (A), the hole remains at the $1S_h$ level, as shown in Figure 3AI. Therefore the electronic coupling strength *H(R),* depends on the wavefunction overlap between the QD 1S electron level and molecular LUMO, and can be assumed to be proportional to the amplitude of the 1S electron density at the QD surface, i.e. $|H(R)|^2 = C_H|\Psi_{1Se}(R)_0|^2$, where C_H is a size independent factor that depends on the QD material and molecule.[31] With these approximations, the nonadiabatic ET rate from the QD to adsorbate can be described by Marcus ET theory:[10]

$$k_{ET}(R) = C_H \frac{2\pi}{\hbar} \frac{|\Psi_{1\mathrm{Se}}(\mathrm{R})_0|^2}{\sqrt{4\pi\lambda k_B T}} \exp[-\frac{(\lambda+\Delta \mathrm{G}(\mathrm{R}))^2}{4\lambda \mathrm{k_B T}}] \qquad (1)$$

where ΔG is the free energy change and λ the total reorganization energy for ET between the reactant and product state.

The 1S electron density at the QD surface, $\Psi_{1\mathrm{Se}}(\mathrm{R})_0$, can be calculated using an effective mass model, as described in SI1. The values of ΔG for each QD-acceptor complex calculated for different QD sizes are listed in Table SI2. They reflect the difference in electron energy in the acceptor and QD 1S level, and the change in electron-hole Coulomb interaction and charging energies, as described in the supporting information (SI6). Because of the difference in the molecules' redox potentials, the driving force (-ΔG) for ET from the QDs to these acceptors follows the order of MB^+ (1.31 ~ 0.72 ev) > MV^{2+} (0.84 ~ 0.42 eV) >AQ (0.61 ~ 0.04 eV). The total reorganization energy (λ) for the QD-acceptor complexes in heptane is estimated to be about 200 ~ 500 meV (SI6). It contains the estimated contributions of inner sphere reorganization of the acceptor (~100-300 meV) and solvent reorganization (~100-200 meV), with negligible contribution from the QD[19,36]. With these values of $\Psi_{1Se}(R)_0$, $\Delta G(R)$ and λ, the ET rate constants as a function of QD size can be calculated according to Eq. 1. The calculated rates with λ = 400 meV are shown in Figure 2 upper panel (A, B, C), where the amplitudes have been rescaled for comparison with experimental results (qualitatively similar results are obtained for λ in the 200 ~ 500 meV range).

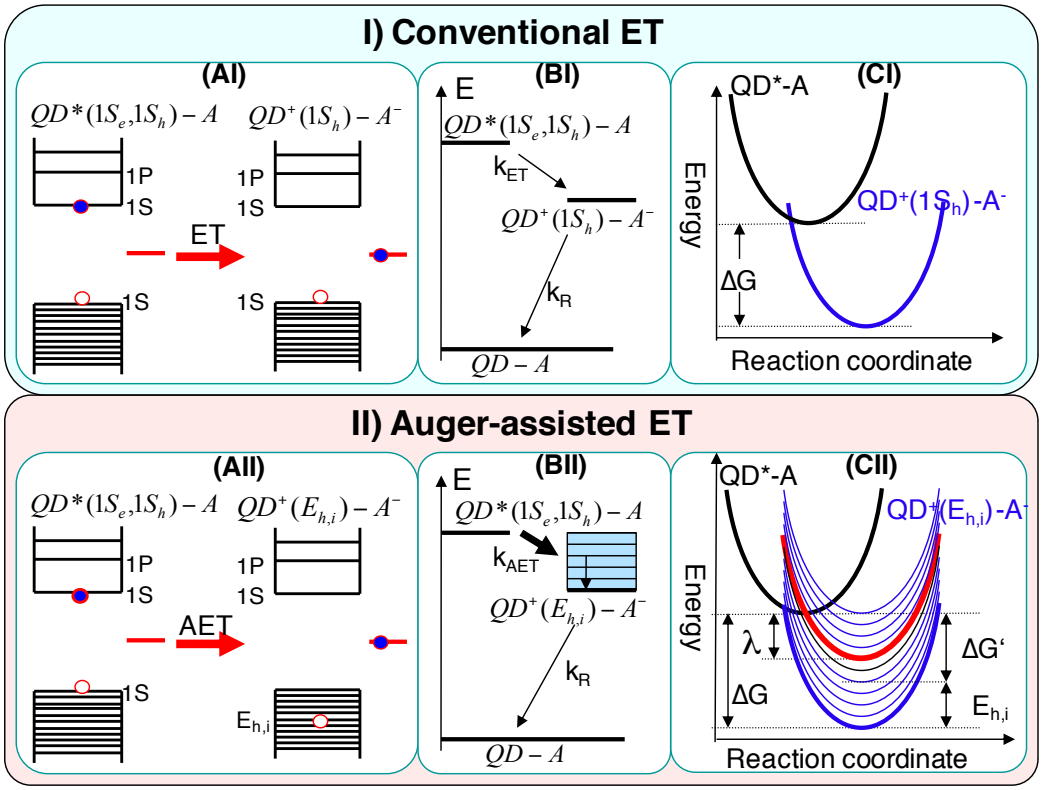

Figure 3. Conventional (i=I, upper panel) and Auger-assisted (i=II, lower panel) models for ET from QDs. (Ai) Single particle picture, showing the electron and hole levels before and after the ET process. In conventional ET(AI), the 1S electron is transferred from QD* ($1S_e$) to the electron acceptor (A) without changing the hole level ($1S_h$). In Auger-assisted ET(AII), ET can be coupled with a change in the hole energy level, giving rise to a continuum of product states, each corresponding to the hole in a different excited level. (Bi) State representation showing the energy of the ground (QD-A), excited (QD*-A) and charge-separated states (QD^+-A^-) as well as the ET (with rate k_{ET} or k_{AET}) and back ET (k_R) processes. (Ci) Marcus representation showing the energy of the reactant and product states as a function of the nuclear displacement along the ET coordinate. (Di) Calculated ET rates as a function of driving force at indicated reorganization energies for conventional (i=I) and Auger assisted (i=II) models.

As shown in Figure 2 upper panel, for all QD-acceptor complexes the observed ET rates increase at decreasing QD sizes (or increasing driving force). For ET from CdS and CdSe QDs to AQ molecules, the estimated -ΔG values (0.04 ~ 0.31 eV) are smaller than λ, falling in the Marcus normal regime, and the observed size dependence of the ET rates can be qualitatively described by the conventional ET model.[10] ET from CdS or CdSe QDs to MB^+ and from CdTe QDs to MB^+ and MV^{2+} molecules, for which the -ΔG values (0.67 ~ 1.31 eV) significantly exceed λ, is in the Marcus inverted regime (Figure 2DI and Figure 3 upper panel), where the conventional ET model predicts a slower ET rate with decreasing size (increasing driving force), in strong disagreement with the experiment.

In the conventional ET model, we have assumed that the electron transfer is independent from the hole dynamics. This assumption has been shown to be often inadequate in QDs, in which the enhanced Coulomb interaction has led to correlated electron and hole dynamics, such as Auger-assisted hot carrier thermalization and multicarrier Auger recombination.[8,37-40] We propose an Auger-assisted ET model, as depicted in Figure 3AII, in which the excess electron energy (the energy difference between the 1S level and the acceptor LUMO) can also be conserved by the excitation of 1S holes to a deeper level with energy $E_{h,i}$ below the 1S hole, in addition to the vibrations of the lattice and acceptor molecules. The excited hole can then relax efficiently within the densely spaced valance band levels.[41] Because of the quasi-continuum nature of the hole states in these QDs, instead of one product state ($QD^+[1S_h]$-A^-) involved in the conventional ET model, there is a manifold of product states ($QD^+[E_{h,i}]$-A^-), corresponding to the excitation of the hole to different levels ($E_{h,i}$) (Figure 3BII and CII). In the non-adiabatic limit, the total ET rate is the sum of Auger-assisted ET rates to these product states, which is given by:

$$k_{AET}(R) = \sum_i k_{AET}(R, E_{h,i}) = \sum_i \frac{2\pi}{\hbar} \frac{\left|H_{AET}(R,E_{h,i})\right|^2}{\sqrt{4\pi\lambda k_B T}} \exp[-\frac{(\lambda+\Delta G'(R,E_{h,i}))^2}{4\lambda k_B T}] \quad (2)$$

The driving force for Auger-assisted ET $\Delta G'(R, E_{h,i}) = \Delta G(R) + E_{h,i}$ is smaller than that for the conventional ET, ΔG (referred to as the apparent driving force), by the amount of hole excitation energy ($E_{h,i}$). The electronic coupling strength, $H_{AET}(R,E_{h,i})$, depends not only on the overlap of the 1S electron and acceptor orbitals (as in conventional ET), but also on the electron - hole Coulomb interaction, which is inversely proportional to the QD radius R.[17,42] We further assume that the dense hole levels in CdX QDs can be described by a quasi-continuum with a density of states (DOS) $\rho_h(E_h, R)$ and the electronic coupling matrix element is independent of the hole energy level. As shown in Figure S6, for CdSe QDs of different radius (between 0.8-2 nm), the calculated DOS of the quasi-continuous valence band states within 1eV from the band edge increases linearly with hole energy and QD volume and can be well represented by $\rho_h(E_h, R)dE_h \propto E_h R^3 dE_h$. Thus, the total ET rate to all product states can be simplified to:

$$k_{AET}(R) = C|\Psi_{1Se}(R)_0|^2 R^2 \int_{E_h=0}^{\infty} dE_h E_h \frac{2\pi}{\hbar} \frac{1}{\sqrt{4\pi\lambda k_B T}} \exp[-\frac{(\lambda+\Delta G(R)+E_h)^2}{4\lambda k_B T}] \quad (3)$$

The ET rates calculated according to the Auger-assisted model (Eq. 3) with λ = 400 meV are shown in Figure 2AII, BII and CII. The calculated rates for each QD-acceptor series have been scaled by a common scaling factor for better comparison with our experimental values. The predicted size dependence of Auger-assisted ET rates agrees well with the measured trends for all QDs and acceptors.

The key difference between the conventional and Auger-assisted ET models is dramatically different dependences on the driving force in the Marcus inverted regime, as shown in Figure 2DI and DII. To more clearly illustrate this dependence, we define scaled ET rates, in which the size and material dependent coupling strength can be removed and only the driving

force dependence remains. The scaled rates for the conventional, $k'_{ET}(\Delta G)$, and Auger-assisted, $k'_{AET}(\Delta G)$, ET processes are:

$$k'_{ET}(\Delta G) = \frac{k_{ET}(R)}{C_H|\Psi_{1Se}(R)_0|^2} = \frac{2\pi}{\hbar}\frac{1}{\sqrt{4\pi\lambda k_B T}}\exp[-\frac{(\lambda+\Delta G(R))^2}{4\lambda k_B T}] \quad (4)$$

$$k'_{AET}(\Delta G) = \frac{k_{AET}(R)}{C|\Psi_{1Se}(R)_0|^2 R^2} = \int_{E_h=0}^{\infty} dE_h E_h \frac{2\pi}{\hbar}\frac{1}{\sqrt{4\pi\lambda k_B T}}\exp[-\frac{(\lambda+\Delta G(R)+E_h)^2}{4\lambda k_B T}] \quad (5)$$

Shown in Figure 2DI and DII are the measured scaled ET rate constants as a function of driving force. To obtain these rates, the measured rate constants were divided by the size and material dependent scaling factor, $C_H|\Psi_{1Se}(R)_0|^2$ and $C|\Psi_{1Se}(R)_0|^2R^2$ for the conventional (Figure 2DI) and Auger-assisted (Figure DII) ET models, respectively. One common C_H and C factors are chosen for each series of QD-acceptor complexes (of different QD sizes) to account for the material dependent coupling strength. These factors are chosen such that QD-acceptor complexes with the same driving force have the same ET rates, as defined in Eq. 4 and 5, regardless of their sizes and materials. It can be seen from Figure 2DI and 2DII, when -ΔG is small (< 0.4 eV), the logarithm of the scaled ET rates show a steep rise with increasing driving force; and when -ΔG exceeds ~ 0.4 eV, it increases more slowly with the driving force.

To compare with the experimental values, the scaled ET rates for the conventional and Auger-assisted ET models are calculated according to Eq. 4 and 5, respectively, using λ values of 0.3, 0.4 and 0.5 eV. For conventional ET model, as predicted by the Marcus theory, with increasing driving force, the ET rate increases in the normal regime (-ΔG < λ), reaches a maximum (at -ΔG = λ), and decreases in the inverted regime (-ΔG > λ), contrary to the experimental results (Figure 4A). For Auger-assisted ET model, the predicted rates increase with the driving force at -ΔG < λ, similar to the conventional ET model. However, the Auger-assisted

ET rate continues to increase with driving force in the inverted regime ($-\Delta G > \lambda$), in qualitative agreement with the experimental results.

The origin for the lack of Marcus inverted regime behavior in Auger-assisted ET model can be attributed to the presence of the continuum of product states, to which ET can occur with effective driving forces ($-\Delta G'$) ranging from 0 (hole excitation takes all the free energy change) to $-\Delta G$ (hole is not excited) and corresponding activation barriers of $(\lambda+\Delta G')^2/4\lambda$. When the apparent driving force ($-\Delta G$) is larger than λ, the rate for the pathway with no hole excitation (the conventional pathway) decreases due to increasing activation barrier. However, there exist Auger-assisted activationless reaction channels where the effective driving force $-\Delta G' = (-\Delta G) - E_h$ is close to λ, and ET process is barrier-less. We denote the regime where $-\Delta G > \lambda$ as Auger assisted regime (Figure 3DII), because ET occurs most effectively with the excitation of holes, overcoming the unfavorable Frank-Condon overlap in the Marcus inverted regime in the conventional ET pathway.

For intramolecular ET processes, the unfavorable Frank-Condon overlap in the Marcus inverted regime can also be reduced by ET to excited states of the reduced molecular acceptors,[43] or by the excitation of high frequency vibration modes.[12,44] In QD-acceptor complexes, the electron-hole Coulomb interaction within the QDs are in the 130-260 meV range (R= 1~2 nm, depending on size), which is much larger than the QD-adsorbate interaction (estimated to be less 10 meV from the shift of QD 1S exciton band upon adsorbate binding), suggesting that the Auger-assisted pathway is the most-likely mechanism. This is supported by previous studies of hot-electron relaxation in QDs, which have shown that Auger cooling is much faster than relaxation via excitation of surface ligand vibrations and lattice phonons.[37,38,45-47] A direct experimental proof of the Auger-assisted ET pathway would require the observation of hole

excitation. Unfortunately, hot holes in CdX (X=S, Se and Te) QDs relax back to the band edge on the subpicosecond time scales,[41,45] which is faster than the ET time observed in this experiment. Therefore, direct observation of hole excitation is not possible. Another experimental proof would be measuring the driving force dependence of electron transfer rates from QDs in the absence of holes. However, this is also difficult to realize experimentally. Using the hole accepting molecules we know, including thiols and phenothiazine, the hole removal time (typically on the order of hundreds of picosecond to nanosecond[7,48-50]) is too slow to compete with the interfacial electron transfer process, especially for those in the Auger-assisted regime. Furthermore, previous experimental and theoretical evidence also suggests that trapped carriers on QD surface can also be involved in Auger recombination process.[40,51] To provide further evidence to support the proposed mechanism, we have turned to computational modeling of the ET processes in QD-acceptor complexes.

The first computational study is performed using time-domain density functional theory combined with nonadiabatic molecular dynamics, as explained in SI10. The system comprises a $Cd_{33}Se_{33}$ QD in contact with the MB^+ molecule (Figure S7 and S8). Photo-excitation promotes an electron from the QD HOMO to the QD LUMO, leaving a hole in the HOMO orbital. The details of the Auger-assisted ET process are illustrated in Figure 4(a), which shows the time evolution of the energies of various parts of the system along a representative trajectory. During ET, the electron energy decreases on a picosecond timescale, indicating the transfer of the electron from QD LUMO to MB^+ LUMO. At the initial stage, the energy lost by the electron is gained exclusively by the hole, confirming the proposed Auger-assisted ET mechanism. The hole never gains the full ΔG of energy lost by the electron, because the hole energy is dissipated by phonons, which is evident in the anti-correlated decrease of hole energy and increase of phonon

energy at longer time. Figure 4(b) shows the calculated Auger-assisted ET rates as a function of $-\Delta G$ values from 0.75 to 1.35 eV. These results are averages over multiple nuclear trajectories at a given ΔG value. With increasing $-\Delta G$, the Auger ET rate increases slightly. In contrast, conventional ET processes (where the hole is fixed at the QD HOMO) exhibit an order of magnitude slower ET rates that *decrease* with increasing $-\Delta G$, showing the expected Marcus inverted regime behavior. Therefore, our *ab initio* results confirm that the Auger excitation of the hole eliminates the Marcus inverted region, in agreement with our experimental result.

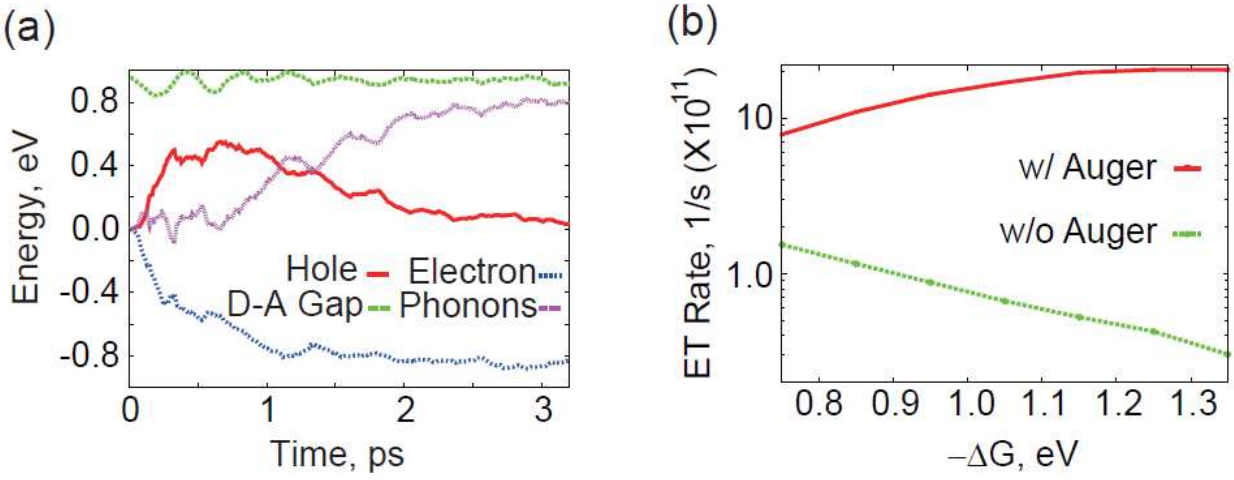

Figure 4. Time-domain *ab initio* modeling of Auger-assisted ET from CdSe QD to MB. **(a)** Time evolution of the electron, hole and phonon energies, and the donor-acceptor energy gap (ΔG). The excess energy generated by the ET is accommodated by the excitation of hole, which is promoted from the QD HOMO to deeper VB orbitals. Later, the hole relaxes by coupling to phonons. **(b)** Calculated ET rates as a function of driving force ($-\Delta G$) for Auger-assisted and conventional ET processes.

The direct *ab initio* dynamics simulation described above is limited to small particles. Auger-assisted electron trapping times for QDs with sizes in our experimental range (R=1.02, 1.46 and 1.92 nm) have therefore been performed using the semiempirical pseudopotential method. Electron transfer from QD to adsorbates transforms a delocalized conduction band electron to a localized electron at the molecule. We mimic this process by considering the transfer of an electron from the QD LUMO to a surface trap whose energy coincides with that of the MB LUMO. The details of the calculation can be found in SI11. The calculated electron trapping times increase with increasing dot size, in agreement with the experimental findings (see Fig. S9 and S10). The transfer times for ET not accompanied by the excitation of the hole are about three orders of magnitude longer (i.e., a few nanoseconds or longer) than those with hole excitation, supporting the proposed Auger assisted ET pathway.

Our study reveals a photoinduced electron transfer pathway from QDs that is fundamentally different from those in molecular chromophores and bulk semiconductor. Because Auger-type processes occur in most quantum confined nanomaterials (QDs, quantum rods, nanowires, carbon nanotudes, graphenes…), we believe that the Auger assisted ET model proposed for CdX QDs herein should be generally applicable for describing exciton dissociation in other excitonic nanomaterials.

Supporting Information. Sample preparation and characterization, effective mass modeling, transient absorption spectra and kinetics, free energy and reorganization energy estimate, hole DOS calculation, time-domain ab initio simulation and atomistic semiempirical pseudopotential calculation. This material is available free of charge via the Internet at http://pubs.acs.org.

Corresponding Author

*Email: tlian@emory.edu

Acknowledgements

We acknowledge the financial supports from the Office of Basic Energy Sciences of the US Department of Energy (grant No. DE-FG02-12ER16347 to TL, and DE-SC0006527 to OVP), KAKENHI grant No. 24750016 (to KHD), and the Royal Society under the URF scheme (To MC).

References

(1) Han, Z.; Qiu, F.; Eisenberg, R.; Holland, P. L.; Krauss, T. D. *Science* **2012**, *338*, 1321.

(2) Sambur, J. B.; Novet, T.; Parkinson, B. A. *Science* **2010**, *330*, 63.

(3) Tisdale, W. A.; Williams, K. J.; Timp, B. A.; Norris, D. J.; Aydil, E. S.; Zhu, X.-Y. *Science* **2010**, *328*, 1543.

(4) De Volder, M. F. L.; Tawfick, S. H.; Baughman, R. H.; Hart, A. J. *Science* **2013**, *339*, 535.

(5) Semonin, O. E.; Luther, J. M.; Choi, S.; Chen, H.-Y.; Gao, J.; Nozik, A. J.; Beard, M. C. *Science* **2011**, *334*, 1530.

(6) Zhu, H.; Lian, T. *Energy Environ. Sci.* **2012**, *5*, 9406.

(7) Zhu, H.; Song, N.; Lv, H.; Hill, C. L.; Lian, T. *J. Am. Chem. Soc.* **2012**, *134*, 11701.

(8) Zhu, H.; Yang, Y.; Lian, T. *Acc. Chem. Res.* **2013**, *46*, 1270.

(9) Marcus, R. A. *J. Chem. Phys.* **1956**, *24*, 966.

(10) Marcus, R.; Sutin, N. *Biochim. Biophys. Acta* **1985**, *811*, 265.

(11) Closs, G. L.; Miller, J. R. *Science* **1988**, *240*, 440.

(12) Barbara, P. F.; Meyer, T. J.; Ratner, M. A. *J. Phys. Chem.* **1996**, *100*, 13148.

(13) Miller, J. R.; Calcaterra, L. T.; Closs, G. L. *J. Am. Chem. Soc.* **1984**, *106*, 3047.

(14) Akesson, E.; Walker, G. C.; Barbara, P. F. *J. Chem. Phys.* **1991**, *95*, 4188.

(15) Marcus, R. A. *J. Chem. Phys.* **1965**, *43*, 679.

(16) Brus, L. E. *J. Chem. Phys.* **1983**, *79*, 5566.

(17) Brus, L. E. *J. Chem. Phys.* **1984**, *80*, 4403.

(18) Cánovas, E.; Moll, P.; Jensen, S. A.; Gao, Y.; Houtepen, A. J.; Siebbeles, L. D. A.; Kinge, S.; Bonn, M. *Nano Lett.* **2011**, *11*, 5234.

(19) Tvrdy, K.; Frantsuzov, P. A.; Kamat, P. V. *Proc. Natl. Acad. Sci.* **2011**, *108*, 29.

(20) Žídek, K.; Zheng, K.; Ponseca, C. S.; Messing, M. E.; Wallenberg, L. R.; Chábera, P.; Abdellah, M.; Sundström, V.; Pullerits, T. *J. Am. Chem. Soc.* **2012**, *134*, 12110.

(21) Asbury, J. B.; Hao, E.; Wang, Y. Q.; Ghosh, H. N.; Lian, T. Q. *J. Phys. Chem. B* **2001**, *105*, 4545.

(22) She, C. X.; Anderson, N. A.; Guo, J. C.; Liu, F.; Goh, W. H.; Chen, D. T.; Mohler, D. L.; Tian, Z. Q.; Hupp, J. T.; Lian, T. Q. *J. Phys. Chem. B* **2005**, *109*, 19345.

(23) Huang, J.; Stockwell, D.; Huang, Z.; Mohler, D. L.; Lian, T. *J. Am. Chem. Soc.* **2008**, *130*, 5632.

(24) Kamat, P. V.; Dimitrijevic, N. M.; Fessenden, R. W. *J. Phys. Chem.* **1987**, *91*, 396.

(25) Yang, Y.; Rodríguez-Córdoba, W.; Lian, T. *J. Am. Chem. Soc.* **2011**, *133*, 9246.

(26) Bird, C. L.; Kuhn, A. T. *Chem. Soc. Rev.* **1981**, *10*, 49.

(27) Cao, Y.; Rabinowitz, D. J.; Dixon, D. W.; Netzel, T. L. *Synthetic Commun.* **2009**, *39*, 4230

(28) Yu, W. W.; Qu, L. H.; Guo, W. Z.; Peng, X. G. *Chem. Mater.* **2003**, *15*, 2854.

(29) Morris-Cohen, A. J.; Frederick, M. T.; Cass, L. C.; Weiss, E. A. *J. Am. Chem. Soc.* **2011**, *133*, 10146.

(30) Huang, J.; Huang, Z.; Yang, Y.; Zhu, H.; Lian, T. *J. Am. Chem. Soc.* **2010**, *132*, 4858.

(31) Zhu, H.; Song, N.; Lian, T. *J. Am. Chem. Soc.* **2010**, *132*, 15038.

(32) Zhu, H.; Song, N.; Lian, T. *J. Am. Chem. Soc.* **2011**, *133*, 8762.

(33) Zhu, H.; Song, N.; Rodríguez-Córdoba, W.; Lian, T. *J. Am. Chem. Soc.* **2012**, *134*, 4250.

(34) Song, N.; Zhu, H.; Jin, S.; Zhan, W.; Lian, T. *ACS Nano* **2011**, *5*, 613.

(35) Song, N.; Zhu, H.; Jin, S.; Lian, T. *ACS Nano* **2011**, *5*, 8750.

(36) Tisdale, W. A.; Zhu, X.-Y. *Proc. Natl. Acad. Sci.* **2011**, *108*, 965.

(37) Efros, A. L.; Kharchenko, V. A.; Rosen, M. *Solid State Commun.* **1995**, *93*, 281.

(38) Klimov, V. I.; Mikhailovsky, A. A.; McBranch, D. W.; Leatherdale, C. A.; Bawendi, M. G. *Phys. Rev. B* **2000**, *61*, R13349.

(39) Klimov, V. I.; Mikhailovsky, A. A.; McBranch, D. W.; Leatherdale, C. A.; Bawendi, M. G. *Science* **2000**, *287*, 1011.

(40) Cohn, A. W.; Schimpf, A. M.; Gunthardt, C. E.; Gamelin, D. R. *Nano Lett.* **2013**, *13*, 1810.

(41) Cooney, R. R.; Sewall, S. L.; Anderson, K. E. H.; Dias, E. A.; Kambhampati, P. *Phys. Rev. Lett.* **2007**, *98*, 177403.

(42) Klimov, V. I.; McBranch, D. W. *Phys. Rev. Lett.* **1998**, *80*, 4028.

(43) Petersson, J.; Eklund, M.; Davidsson, J.; Hammarström, L. *J. Phys. Chem. B* **2010**, *114*, 14329.

(44) Jortner, J. *J. Chem. Phys.* **1976**, *64*, 4860.

(45) Hendry, E.; Koeberg, M.; Wang, F.; Zhang, H.; de Mello, D.; aacute; C.; Vanmaekelbergh, D.; Bonn, M. *Phys. Rev. Lett.* **2006**, *96*, 057408.

(46) Cooney, R. R.; Sewall, S. L.; Dias, E. A.; Sagar, D. M.; Anderson, K. E. H.; Kambhampati, P. *Phys. Rev. B* **2007**, *75*, 245311.

(47) Pandey, A.; Guyot-Sionnest, P. *Science* **2008**, *322*, 929.

(48) Huang, J.; Huang, Z.; Jin, S.; Lian, T. *J. Phys. Chem. C* **2008**, *112*, 19734.

(49) Wuister, S. F.; Donega, C. D.; Meijerink, A. *J. Phys. Chem. B* **2004**, *108*, 17393.

(50) Liu, I. S.; Lo, H. H.; Chien, C. T.; Lin, Y. Y.; Chen, C. W.; Chen, Y. F.; Su, W. F.; Liou, S. C. *J. Mater. Chem.* **2008**, *18*, 675.

(51) Califano, M. *J. Phys. Chem. C* **2008**, *112*, 8570.

For TOC Only

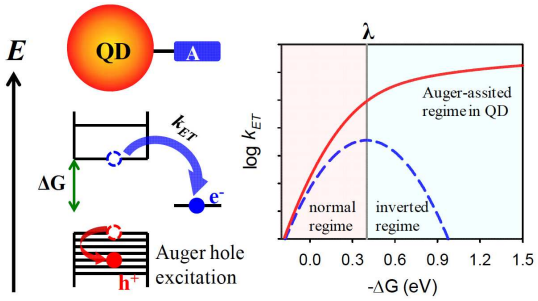
E
QD
A
k_{ET}
ΔG
e⁻
h⁺
Auger hole
excitation
λ
log k_{ET}
Auger-assited
regime in QD
normal
regime
inverted
regime
0.0
0.3
0.6
0.9
1.2
1.5
-ΔG (eV)